CrystEngComm

Accepted Manuscript

ROYAL SOCIETY OF CHEMISTRY

www.rsc.org/crystengcomm

Cite this: DOI: 10.1039/c0xx00000x

www.rsc.org/xxxxxx

ARTICLE TYPE

Hydrothermal growth of ZnO nanorods on Zn substrates and their application in degradation of azo dyes under ambient conditions

Xiaoyan Cai,[a] Bingqian Han,[a] Shaojuan Deng,[a] Yan Wang,[a] Chengjun Dong ,[a] Yude Wang,*[a,b] and Igor Djerdj*[c]

Received (in XXX, XXX) Xth XXXXXXXXX 20XX, Accepted Xth XXXXXXXXX 20XX
DOI: 10.1039/b000000x

A new type of catalytic material, large-scaled ZnO nanorod arrays grown on self-source substrate, was directly synthesized by a facile hydrothermal approach. The catalytic activity of the ZnO nanocrystals with different exposed surfaces, including ZnO hexagonal nanorods with exposed reactive {0001} facets, hexagonal ZnO nanopyramids with the nonpolar {01 1 0} planes, and pencil-like morphology with exposed {10$\bar{1}$1} polar planes, was tested towards the degradation of the azo dyes (Congo red (CR) and methyl orange (MO)). The aqueous azo dyes can be degraded efficiently under ambient conditions, requiring neither light illumination nor additional energy (agitation, ultrasonic, etc.). Systematic experiments suggested that the dye degradation proceeds through the electron transfers from the anionic dye molecules to the catalyst and then to electron acceptors such as dissolved oxygen. It strongly depends on the exposed polar surfaces of the ZnO nanocrystals, giving rise to the relative higher catalytic activity and stability of the ZnO hexagonal nanopencils. The present ZnO nanorods arrays grown on Zn substrate requires no additional reagents or external energy input, which hence provides a potentially low-cost alternative for the remediation of azo-dye effluents.

1. Introduction

At present times, azo dyes are one of the largest groups of colorants used in industries like textiles, dyestuff, etc.[1,2] They are the copious source of coloured organics emanating as a waste from the industry dyeing process. These colored dye effluents pose an enormous threat to the environment by releasing toxic and potential carcinogenic substances into the aqueous systems. Several studies of biological, physical and chemical treatment methods have been carried out for the elimination or mineralization of organic azo dyes from wastewater in order to minimize their impact towards environment.[3–6] Among these, biodegradation, adsorption, filtration and ozonation are the most commonly used conventional methods. Each method has its own advantages and disadvantages. For example, aromatic amines from azo dyes are usually resistant to aerobic degradation and carcinogenic compounds may be generated during the anaerobic treatment, in these respects, bio-treatment alone has been found to be ineffective for the colour removal and degradation of dye effluents.[7] The use of adsorption tactic by activated carbon is technically easy but has a high waste disposal cost. While in filtration, only low-molar-mass dyes can pass through the filter system. Although coagulation using alum, ferric salts or lime is a low cost process, the disposal of toxic sludge has also a severe drawback. Lastly, chemical treatment using chlorine or ozone has led to more successful results, but the required high dosages are not found economically feasible.[3]

Recent developments of advanced oxidation processes (AOPs) are of ample interest for the effective oxidation of a wide variety of organics and dyes. UV radiation in the presence of H_2O_2 has yielded encouraging results of color removal from azo-reactive dye containing waters.[8] Amongst them, top priority goes to semiconductor assisted photocatalytic degradation. Unfortunately, the most utilized semiconductor photocatalyst of TiO_2 is active only in the ultraviolet light range due to its wide band gap (3.2 eV for anatase). Although many reports have appeared on modifications of TiO_2 and development of other visible light sensitive photocatalysts,[9,10] the quantum yield is still not satisfying, thus limiting its practical applications.[11] Moreover, TiO_2 has been used in the form of fine powders suspended in water in many applications. Despite the cost of recovery operations and the possible powder loss, recovery of the TiO_2 powders after photocatalytic water treatment is necessary. Nevertheless, it is difficult to maintain the high photocatalytic activity of TiO_2 upon immobilization of TiO_2 powders on a substrate material.[12] It is therefore of great interest to achieve azo dyes degradation that demands neither light illumination (as is the situation of the photocatalytic degradation) nor additional energy (as is the situation in the sonocatalytic degradation).[13,14] Also the need is to develop such a material that acts as an excellent catalyst that can be regenerated or reused multiple times without any significant change in dye removal efficiency and loss in catalyst quantity. Thus, as an alternative option, oxide semiconductor grown on the metal substrate is emphasized as a plausible method in order to decrease the negative effects of dye effluents.

As an important II–VI semiconductor, ZnO is a promising material with fantastic properties and potential applications in numerous fields. Current researches show that ZnO can also be used as a very efficient semiconductor photocatalyst when

compared with TiO_2.[15,16] Lower cost and better performance of ZnO in the degradation of organic molecules have stimulated many researchers to further explore the properties of this oxide in many catalytic degradation reactions.[17,18] Meanwhile, ZnO has emerged as a more efficient catalyst for the destruction of azo-reactive dyes.[19,20] Recently, highly ordered ZnO arrays composed of 1D building blocks exhibited promising perspective for application in multifunctional nanodevices and nanosystems because of their exciting optical and electronic properties, which are closely related to their unique morphologies and spatial organization. However, the researches for application of ZnO nanowire/rod arrays are mostly concentrated in the piezoelectric generator,[21] dye-sensitized solar cells,[22] photonic crystals[23] and super-hydrophobic interface,[24] and ZnO arrays used in dye wastewater treatments are rarely reported. Zhao et al.[25] synthetized ZnO pine-nanotree arrays through hydrothermal route and evaluated its photocatalytic activity by degradation of Rhodamine B (RB), but the ZnO arrays could only degrade low concentration of dye wastewater even under the irradiation of harmful ultraviolet light. Ma et al.[26] reported that the ZnO nanorod arrays grown on a Cu substrate exhibited decent photocatalytic performance in the degradation of methyl orange (MO) under UV light condition, but the ZnO nanorods were peeled off from the substrate and added into wastewater in the form of powder, thus increasing the difficulty of recycling applications. On the other hand, to our best knowledge, the catalytic activity of ZnO arrays of various morphologies, used as a potential catalytic material for the degradation of azo dyes with high concentration from wastewater under the presence or absence of visible light has never been studied nor reported.

Herein we present, for the first time, the implementation of ZnO nanorods grown on Zn substrate as catalysts for the degradation of azo dyes under ambient conditions, requiring neither light illumination nor additional energy (agitation, ultrasonic, etc.). The growth of ZnO arrays on Zn substrate by a simple hydrothermal method was discussed, and the intrinsic characteristics of the resulting catalysts were studied by X-ray diffraction (XRD), scanning electron microscopy (SEM) and X-ray photoelectron spectroscopy (XPS). Congo red (CR) and methyl orange (MO) were used as azo dye solutions for the observation of the degradation property. Also, a new mechanism for the catalytic decomposition in the presence of ZnO nanostructures grown on Zn substrate was proposed.

2. Experimental

Zinc foil (the purity is 99.9%, the thickness is 0.2 mm), sodium hydroxide (NaOH, A.R., Zhiyuan chemical reagent plant of Tianjin, China) and aqueous ammonia ($NH_3 \cdot H_2O$, 25 wt% solution, A.R., Fengchuang chemical reagent plant of Tianjin, China) were used for the preparation of ZnO nanorod arrays.

The metallic zinc foil of dimension 6 cm×2 cm was cleaned in ultrasonic bath first by anhydrous ethanol followed by distilled water for 30 min to remove various pollutants on its surface. A certain An optimal concentration (Table 1) of sodium hydroxide solution or aqueous ammonia solution was poured into a Teflon cup (80 mL) in a stainless autoclave and then ultrasonically washed zinc plate was immersed in the reaction mixture. The ZnO film was prepared by a hydrothermal oxidation of zinc foil in above mentioned alkaline aqueous medium in the temperature ranging between 80~140 ˚C within 12 h. After the completion of reaction, the film was rinsed thoroughly with distilled water several times and dried in air. The experimental conditions for the syntheses performed are summarized in Table 1.

Powder X-ray diffraction (XRD) was carried out with a Rigaku D/MAX-3B powder diffractometer using copper target and Kα radiation (λ = 1.54056 Å). The obtained powder-like data were used for the phase identification, where the diffracted X-ray intensities were recorded in the range from 30° to 80° (2θ) in step of 0.02°. Scanning electron microscopy (SEM) characterization was performed with FEI QUANTA200 microscope operating at 15 kV. X-ray photoelectron spectroscopy (XPS) was carried out at room temperature in ESCALAB 250 system. During XPS analysis, an Al Kα X-ray beam was adopted as the excitation source and the vacuum pressure of the instrument chamber was 1×10^{-7} Pa. Fourier transformed infrared (FTIR) spectra, in the range of 4000–400 cm^{-1}, were recorded on a Perkin–Elmer 2000 FTIR spectrometer.

CR ($C_{32}H_{22}N_6Na_2O_6S_2$, molecular weight: 696.67 g mol^{-1}, from Guangzhou Reagent Corporation, China) and MO ($C_{14}H_{14}N_3NaO_3S$, molecular weight: 327.33 g mol^{-1}, from Shengao chemical reagent plant of Tianjin, China) were used as model dyes to investigate the catalytic activity of the ZnO nanostructures. The lighting conditions during the degradation process (ultraviolet light irradiation, visible light irradiation and dark condition), azo dyes species (CR and MO), initial dyes concentration (10^{-5} M, 10^{-4} M and greater than 10^{-4} M) and degradation time were varied to determine the optimum working conditions for azo dyes degradation. In a typical degradation experiment, ZnO films grown on Zn substrate with the lateral dimensions of 2 cm×2 cm were horizontally placed in the bottom of quartz beakers, and then 40 mL of CR aqueous solutions (CRS) with an initial concentration of 10^{-5} M were introduced. The reaction mixtures were statically placed in the dark, under a visible light irradiation and ultraviolet light irradiation conditions, which was achieved in the black box, with the fluorescent lamp irradiation and UV lamp irradiation, respectively. The degradation was carried out at room temperature and atmospheric pressure, and no additional energy (agitation, ultrasonic, etc.) was provided. During the degradation, three milliliter of the dye solution was continually extracted at a given time and subsequently centrifuged to separate the flocculent precipitates and dye solutions at 4000 rev min^{-1} for 30 min. The concentration (C) of the centrifuged solution and the initial concentration (C_o) of the CR solution were monitored immediately by measuring the absorbance of the supernatant at 498 nm using a spectrophotometer (model no. JH722N). The degradation rate was calculated as C/C_o. ZnO films were simply rinsed with distilled water several times, dried in air and then used as the recycled catalysts to degrade new CR solutions. The flocculent precipitates collected from the decolorized CR solution were

characterized by X-ray diffraction (XRD) and Fourier transform infrared spectroscopy (FTIR).

3. Results and Discussion

3.1. Structural characterization

Fig. 1 shows XRD patterns of the as-grown ZnO crystals on Zn substrates synthesized by hydrothermal reaction in the alkaline solutions at different temperature for 12 h. Before hydrothermal processing, all diffraction peaks of the substrate can be indexed as pure hexagonal Zn of the JCPDS no. 87-0713. It should be noted that the peak at about 36.2° corresponding to the (002) plane in intensity is much more intense than those of all other peaks, suggesting that the Zn seeds are mainly enclosed with the (002) planes. Upon hydrothermal processing for 12 h, the reflections attributed to wurtzite structured ZnO phase of the JCPDS no.80-0075, in addition to those marked with the Zn substrate were detected simultaneously. The existence of two sets of diffraction peaks for sample Z-1, Z-2, Z-3 and Z-4 and no other detected diffraction peaks from impurities prove the successful fabrication of ZnO grown on self-source substrate. The narrow FWHM of the diffraction pattern indicates that the products are of excellent crystal quality. In addition, for sample Z-1 and Z-3, the peak intensity of (002) plane of the ZnO nanostructures are relatively stronger than that of the standard data, suggesting that the wurtzite *c*-axis which is a growth direction of ZnO On the other hand, weak ZnO peaks are observed for sample Z-2 and Z-4, implying that the small amount of ZnO is formed. By comparing samples Z-1 and Z-2, and sample Z-3 and Z-4, it is easy to see that the lower reaction temperature yields to the lower intensity of ZnO related peaks, under the same concentration and category of solution system. The strong reflections corresponding to unreacted zinc indicated that the reaction between zinc and alkaline solution at relatively lower temperature is far from completion.

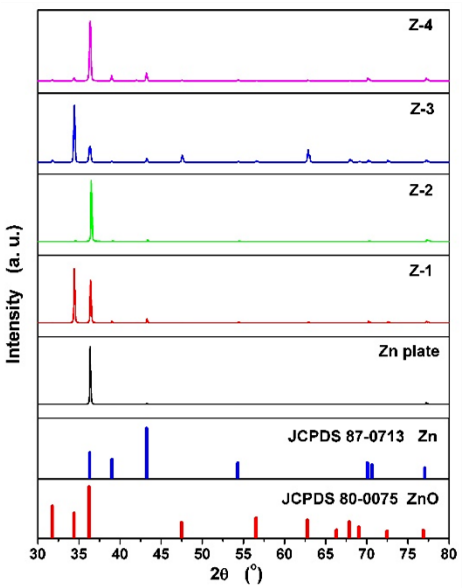

Fig. 1 X-ray diffraction patterns of the ZnO arrays.

For the microstructural analysis the as-synthesized samples were directly transferred to the SEM chamber without disturbing the original nature of the products. The typical SEM images in top view of the ZnO structures grown on Zn substrate are presented in Fig. 2. As it can be seen from Fig. 2(a), the surface of the zinc foil has been coated with quasi-oriented ZnO nanorod arrays, having uniform hexagonal pyramidal-shape with tapering upward from the bottom.

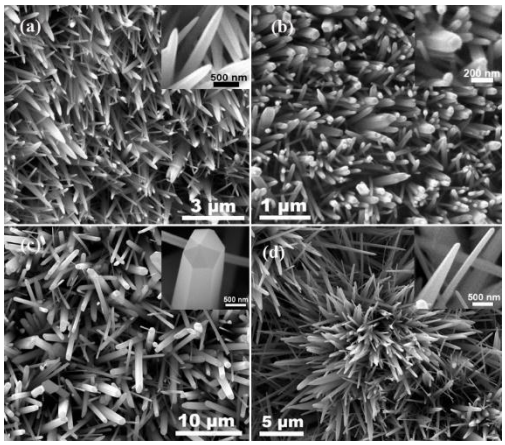

Fig. 2 SEM images of ZnO nanorod arrays: (a) Z-1; (b) Z-2; (c) Z-3; (d) Z-4.

These densely packed arrays of ZnO nanopyramids are grown in 0.6 M of aqueous ammonia solution at 100 °C and their maximum diameter is estimated to be 300 nm. SEM image in Fig. 2(b) reveals that with reducing the reaction temperature from 100 °C to 80 °C whereas keeping other experimental conditions unaltered, the lengths of the achieved nanorods decreased significantly (about 3 and 1 μm for sample Z-1 and Z-2, respectively). The nanorods are almost uniform in length and possess a characteristic hexagonal cross-sectional shape with diameter in the range of approximately 50 to 200 nm. Fig. 2(b) also exhibits that such nanorods have better alignment compared to the previous sample (see Fig. 2(a)), demonstrating the formation of arrays of ZnO nanorods with a preferential growth direction nearly perpendicular to the Zn substrate. When 0.6 M of aqueous ammonia solution is replaced by 1 M of sodium hydroxide solution, the surface morphologies of the ZnO films are significantly different. In Fig. 2(c), an abundant number of free-standing nanorods are observed from the surface of the substrate preserved at NaOH solution with a temperature of 140 °C. It is not hard to notice that the nanorods have a diameter varying from 100 nm to 1 μm and a length of several micrometers, even longer than 10 μm. In addition, as an obvious characteristic property of the as obtained rod arrays, all the tips are contracted with six regular faces of {10$\bar{1}$1} (inset of Fig. 2(c)), which are more approximate pencil-like instead of pyramid-like shape. Fig. 2(d) is attributed to the sample Z-4 with 100 °C reaction temperature and it shows that a collection of ZnO nanorods tend to form cluster-like morphology in a flower shape. Furthermore, the nanorods gathered into the clusters are not uniform throughout their lengths, where most of them are similar with sample Z-1 in

shape, yet have a higher aspect ratio of ~50 (the number is ~10 for sample Z-1). Illustrations displayed in top right corners of Fig. 2(a)-(d) provide insight into the morphological and structural features of a single nanorod. They depict clearly that whether pyramid-like or pencil-like morphology dominates in as obtained material.

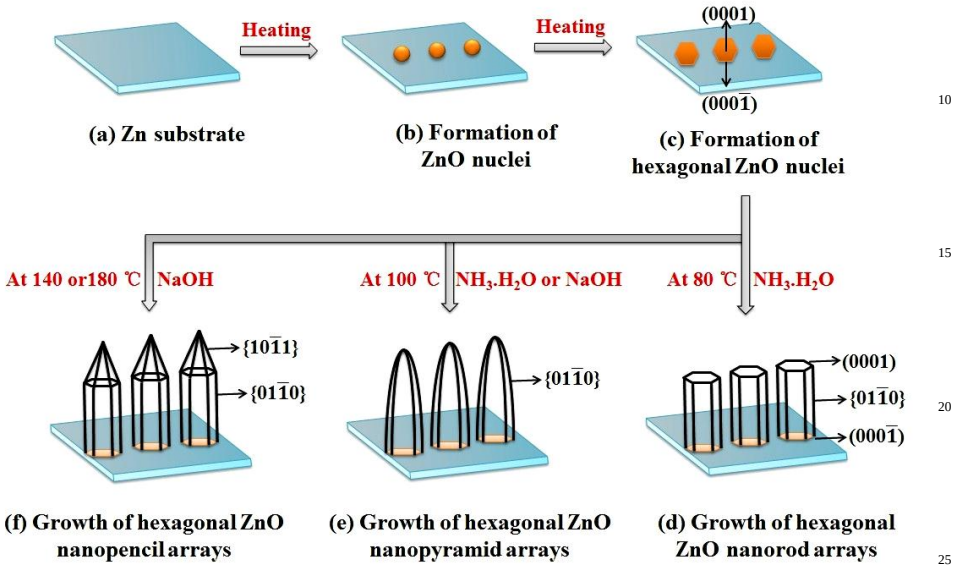

Fig. 3 Schematic illustration of the possible growth mechanism for the formation of different ZnO arrays grown at different reaction conditions.

Further investigation is carried out to see the effect of the reaction temperature on the morphology and the degree of alignment of the nanorods. For this purpose the solution system is kept constant with 1 M of NaOH solution. Fig. S1 (Supp. Inf.) represents the corresponding SEM images of the products. The products formed at 180, 140, 100 and 80 ˚C are shown in Fig. S1(a), 2(c), 2(d) and S1(b) respectively. These images reveal that the nanorods obtained at 180 and 140 ˚C are almost identical, whereas the nanorods obtained at 100 ˚C are more slender in diameter and they are fully aligned relative to other two samples produced at higher temperatures. Nevertheless, in general, the nanorods produced in NaOH solution are found to have more random alignment than those produced in $NH_3 \cdot H_2O$ solution. Obviously, the surface atoms of Zn foil would not get enough energy to form ZnO nuclei in the condition of 80 ˚C sodium hydroxide solution, letting alone further growth, consequently resulting in mild surface corrosion as shown in Fig. 2(d).

The detailed microstructures of the ZnO rod-like structures are investigated using TEM. Typical TEM images in lateral view of the ZnO nanorods broken from substrates (insets of Fig. S2 in Supp. Inf.) present the pointed ends for sample Z-1, Z-3 and Z-4, and the flat end for sample Z-2, respectively. It is clear that the morphologies of the samples are in accordance with the results of the SEM. HRTEM images amplified from the regions marked in red reveal clear crystalline boundaries and lattice fringes of 0.26 ± 0.02 nm, which agree well with the (0001) plane of wurtzite ZnO, and indicate the [0001] growth direction of all the ZnO rods. The SAED patterns shown in the insets further confirm the single-crystal nature of the nanorods grown along *c*-axis. In addition, it can be seen from insets of Fig. S2(c) that the edge of the sharp tip is perpendicular to [01$\bar{1}$1] direction, demonstrating the existence of {10$\bar{1}$1} crystal faces at the top of ZnO nanopencil.

3.2. Growth mechanism of ZnO nanorods

The detailed growth process of the ZnO nanostructures in our synthetic process can be understood on the basis of reactant species and the crystallographic habits of wurtzite hexagonal ZnO. A schematic diagram for the systematic growth of ZnO nanostructure arrays by the hydrothermal reaction process described basing on the study conducted by Q. Ahsanulhaq et al.[27] is shown in Fig. 3. The simple chemical reactions that account for the ZnO growth are inferred as follows:[28,29]

$$Zn + 2H_2O + 4NH_3 \rightarrow [Zn(NH_3)_4](OH)_2 + H_2 \quad (1)$$

$$[Zn(NH_3)_4](OH)_2 \rightarrow ZnO + H_2O + 4NH_3 \quad (2)$$

$$Zn + 2OH^- \rightarrow ZnO_2^{2-} + H_2 \quad (3)$$

$$ZnO_2^{2-} + H_2O \rightarrow ZnO + 2OH^- \quad (4)$$

During the synthesis, Zn atoms in zinc foil react with ammonia molecules or OH^- ions in alkali solution, in which Zn atoms surmount the surface energy of zinc foil, forming ZnO nuclei through hydrolysis reaction (Fig. 3(b)). The ZnO nuclei formed are the building blocks for the formation of the final products. Due to the crystal nature of ZnO, the nuclei have a hexagonal shape (Fig. 3(c)). As we all know, wurtzite hexagonal structure ZnO is a polar crystal that has polar and non-polar faces. In such a polar ZnO crystal, a series of Zn^{2+} and O^{2-} are stacked alternately along the c-axis direction, and the top surfaces are Zn-terminated (0001) and are catalytically active, while the bottom surfaces are O-terminated (000$\bar{1}$) and are chemically inert.[30] Polar faces with surface dipoles are thermodynamically less stable than non-polar faces and often undergo rearrangement to minimize their surface energy and also tend to grow more rapidly. Furthermore, the growth depends on the growth

velocities of different planes in the ZnO crystal, and the slowest growing faces determine the morphology of a particular crystal. Under hydrothermal conditions, the growth velocities of the ZnO crystals in different directions are [0001] > [01$\bar{1}$1] > [01$\bar{1}$0] > [01$\bar{1}$1] > [000$\bar{1}$], demonstrating that the polar (0001) faces are the most rapid-growth-rate planes as compared to other growth facets.[31,32] Hence, the most stable crystalline structure of ZnO should be a hexagonal cross-section of prism grown along the c-axis, in which the side faces of the prism consist of six equivalent {01$\bar{1}$0} crystal planes: (10$\bar{1}$0), (1$\bar{1}$00), (0$\bar{1}$10), ($\bar{1}$010), ($\bar{1}$100) and (01$\bar{1}$0).[33] As observed in Fig. 2(b), the nanorods synthesized in aqueous ammonia at 80 ˚C are consistent with the typical growth habit of ZnO crystal, exhibiting polar Zn-terminated (0001) top and O-terminated (000$\bar{1}$) bottom surfaces and bounded with the six crystallographic non-polar {01$\bar{1}$0} planes (Fig. 3(d)). On the other hand, R.A. Laudise et al.[34] reported that the higher the growth rate, the faster the disappearance of the plane. In contrast to non-polar surfaces, the polar {10$\bar{1}$1} planes usually grow more quickly, forming the crystal shape. Therefore, when the reaction temperature increases at a critical value (equal or greater than 140 ˚C), the high-energy surface disappears and the {10$\bar{1}$1} planes, with higher Miller index and lower surface energy, tend to become preferred due to the electrostatic interaction between the ions and the polar surfaces, resulting in the occurrence of pencil-like ZnO nanostructures (Fig. 3(f)).[27] In case of a modest temperature (100 ˚C), since the surface mobility is not high enough, the behavior that ZnO molecular species deposited at the base and surfaces move to the top of the nanorod arrays is gradually unsustainable, which leads to the nanopyramid morphology as a final product (Fig. 3(e)).

3.3. Removal properties of ZnO nanorods for azo dyes

In general, the catalytic activity is tightly related to the structure of the catalyst.[35] Existing studies showed that morphology and structure affect the catalytic property of ZnO usually by means of small size and high specific surface area.[36] But D. Li et al[37] consider different crystal faces as one of the reasons for the difference in degradation performance. In order to test the catalytic performance of the four ZnO grown structures on Zn substrate denoted with Z-1 to Z-4, the degradation of CR and MO was carried out in an aqueous solution with immersed ZnO nanorods. In order to compare the degradation effects, varying different parameters, such as lighting conditions, initial dye concentration and recycling times, were studied.

The effect of lighting conditions. The results of the CR and MO with concentration of 10^{-5} M degradation in the presence of various ZnO nanorod arrays under different lighting conditions are summarized in a comparative combination plot of Fig. 4, where C_o and C are the initial concentration before reaction and the reaction concentration of the dyes at time t respectively. Fig. 4(a) and (b) show that both CR and MO can be effectively removed by the ZnO nanoarray structures in variety of ambient conditions, including bright and sunless settings. As it is known, ZnO particles can act as photocatalysts and be stimulated by UV-light to generate electron-hole pairs which interact separately with other molecules in water, producing highly oxidative hydroxyl free radicals (·OH) and thus resulting in complete mineralization of many toxic and non-biodegradable organics.[38,39] For this reason, the rapid degradation of azo dyes with UV-light irradiation observed at the beginning of the reaction time can be attributed to photocatalytic activity of ZnO manifested only when activated by ultraviolet with wavelength less than 387 nm. Despite the best removal performance, UV light is harmful to human bodies since it is capable of causing irritation to the skin and eyes, even mutation and carcinogenesis. Thereby the operability of using ZnO nanostructures for degradation of organic wastewater may be reduced and its actual practice for production and living is probably restrained. However, interestingly, ZnO nanorod arrays grown on self-source substrates synthetized via a simple hydrothermal route in our studies are found to have the ability of dislodging CR and MO from aqueous solution under both vis-light illumination and dark conditions without stirring or ultrasound, providing that the duration is long enough, that is, ca. 2-3 days. The removal efficiencies of dyes preserved in the dark are similar to those exposed under a visible light, giving description that the decolouration of dyes by ZnO arrays can be also carried out in the absence of light. This present catalytic degradation will not be subjected to the constraint of time (day and night) and space (indoor and outdoor), which hence provides a potentially low-cost alternative for the remediation of azo-dye effluents. As a supplementary note, no degradation was observed when the dye solution was preserved in the dark or exposed under visible light without any catalyst, while segmental dye could be decomposed when it comes to UV light (not show here).

The effect of initial dyes concentration. A further increase in the dyes concentration is demanded for practical application. The effect of the initial concentration of CR and MO solutions on the catalytic decomposition performance has been studied by varying the concentrations from 10^{-5} M to 10^{-4} M and then greater than 10^{-4} M in the presence of ZnO films with area of 2×2 cm^2 in the dark circumstance. Curves of degradation efficiencies of CR and MO under the different initial concentrations versus time catalyzed by the different ZnO nanostructures are displayed in Fig. S3 (Supp. Inf.). It is obvious that the removal rate depends upon the initial concentration of the azo dyes, where the increased concentration decreases the catalytic efficiency. Also, a longer reaction time is necessary to degrade the higher concentration dyes under the same degradation conditions. It is generally noted that a higher concentration might cause excessive adsorption of the dye molecules on the surface of the adsorbent, giving rise to drastic decrease of adsorption efficiency and fast reached adsorption/desorption equilibrium. However, neither the furious decrease in the degradation activity with dye concentration nor the alleged equilibrium is discovered, proving that the ZnO nanorod-structures act as catalysts instead of adsorbents in our catalytic degradation studies. As seen from Fig. S3(a), degradation rate gradually increase with respect to the treatment time, and CR with low concentration of 10^{-5} M is almost completely degraded by all samples after preservation in the dark for 48 h. Further observations show that, even if the concentration of CR increased exponentially, the corresponding removal efficiency do not decreased exponentially. For instance, in the presence of sample Z-1, 94.6 % of CR with initial concentration of 10^{-5} M is degraded within 48 hours while decoloration rate of 75.6 % is detected when it comes to 10^{-4} M of CR at the same period of time. As another example, in case of

sample Z-4, the consuming time respectively for decomposition of approximately half CR with initial concentration of 10^{-5} M, 10^{-4} M and 1.43×10^{-4} M is 12 h, 36 h and 48 h, rather than corresponding multiple of 12 h, 120 h and 172 h. A possible reason is that the high initial concentration of the dye solution causes more of the degradation reaction to take place to achieve the same level of degradation between the dye molecules and ZnO catalyst.[40] Similar phenomena can be observed in degradation of MO as revealed in Fig. S3(b). By executing vertical comparison of Fig. S3(a) and (b), it is clear that the effect of MO elimination is always slightly behind that of CR, which perhaps on account of the difference between the molecular structures of these two azo dyes. In conclusion, the four ZnO samples have satisfactory ability to degrade both low and high concentration of azo dyes under sunless surroundings, and their excellent degradation performances make them a promising degradation material to remove organic pollutants in industrial wastewater treatments.

The degradation of azo dyes using regenerated ZnO arrays. The stability of catalyst during catalytic reaction is a crucial factor for the practical applications. It is widely accepted that the ZnO semiconductor suffers from serious photoinduced dissolution, which greatly decreases its photocatalytic activity and limits its photocatalytic application.[41] However, photocorrosion of ZnO has been avoided in our study since the catalytic degradation process requires no light illumination.

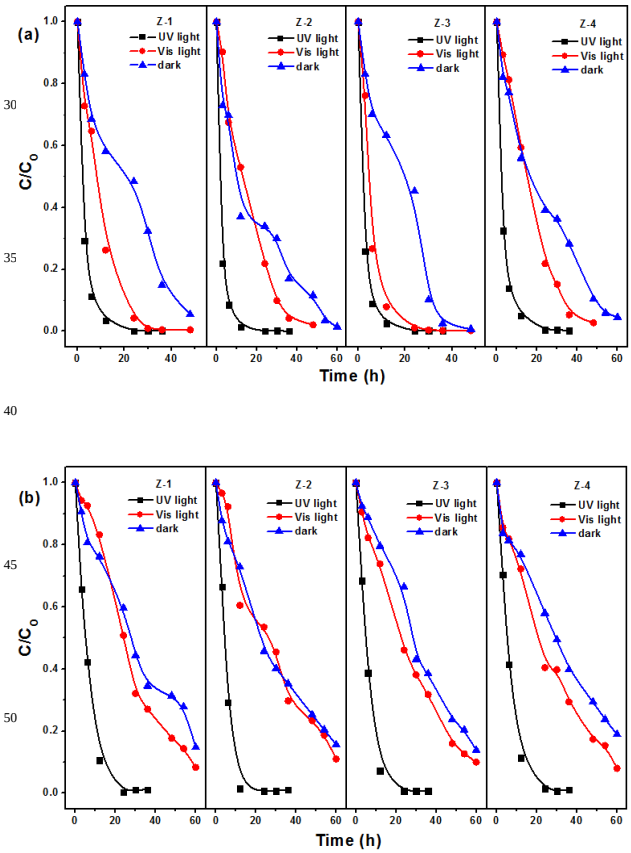

Fig. 4 The comparative degradation rate of azo dyes under different lighting conditions (UV-light irradiation, Vis-light irradiation and dark condition) in the presence of sample Z-1, Z-2, Z-3 and Z-4 (2 cm×2 cm): (a) CR (10^{-5} M, 40 mL); (b) MO (10^{-5} M, 40 mL).

To test the reusability of ZnO nanorod arrays in azo dyes degradation, five cycles of the catalytic decomposition experiment for above as-prepared ZnO samples have been carried out. The ZnO nanostructures after the catalytic reaction were regenerated by simple rinsing with distilled water and drying in air, and the regenerated catalysts were used in the decoloration of new CR and MO under identical dark conditions. As described in Fig. S4(a) (Supp. Inf.), CR with low concentration of 10^{-5} M can be totally decomposed in each cycle and all the ZnO nanostructured materials except sample Z-4 exhibit almost no change in their catalytic activities during the repeated degradation experiments. Sample Z-3 with pencil-like morphology shows the highest stability whereas the catalytic activity of the regenerated ZnO nanopyrimid arrays with relatively poorer orientation (sample Z-4) gradually reduces throughout the recycling tests. On the other hand, the results from Fig. S4(b) show that the catalytic activity of all samples towards 10^{-5} M of MO dye slightly decreases till to the fifth run, and invariably, sample Z-3 is found to exhibit more prominent stability and reusability comparing with any other samples. The degradation efficiencies of high concentration CR and MO by different as-prepared samples, as a function of recycling, are presented in Fig. S4(c) and Fig. S4(d) respectively. It can be perceived that the removed dyes are significantly reduced in the process of recovery as the dye concentration reach up to 10^{-4} M. The reason is possibly being increase in surface deposits during recycling on account of the incomplete removing organic dye molecules remained on the surface leading to reduced reaction sites between catalysts and dye molecules. Curves representing removal efficiency close to each other and no significant difference between them can be noticed at the first cycle. But this uniformity of catalytic capability is not sustainable and hence the curves become dispersed by degrees at the following cycles, giving expression to the differences in terms of reusability. It seems that the catalytic property and stability of ZnO arrays are jointly determined by morphology and orientation. Nevertheless, ignoring the poor stability of sample Z-4 exhibited in the process of circulatory degradation of high concentration MO dye, the smashing performance of other samples especially sample Z-3 is worthy of recognition. The cumulative removal capacity calculated according to Fig. S4(c) and (d) for sample Z-3, the most active and stable catalyst film with area of only 4 cm^2, actually reach up

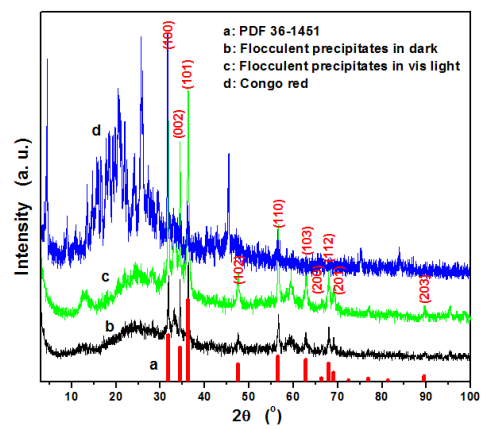

Fig. 5 X-ray diffraction analysis of the flocculent precipitates collected from the degraded CR solutions under different lighting conditions (Vis-light irradiation and dark condition).

Table 1 The major experiments carried out in this work and the mark symbols of the corresponding as-prepared samples.

Mark symbol	Substance of solution system	Concentration of solution system	Volume of solution system	Constant temperature
Z-1	$NH_3 \cdot H_2O$	0.6 M	50 mL	100 ˚C
Z-2	$NH_3 \cdot H_2O$	0.6 M	50 mL	80 ˚C
Z-3	NaOH	1 M	50 mL	140 ˚C
Z-4	NaOH	1 M	50 mL	100 ˚C
Z-5	NaOH	1 M	50 mL	180 ˚C
Z-6	NaOH	1 M	50 mL	80 ˚C

considerable 15.05 mg CR and 5.66 mg MO, respectively. Thus, the higher catalytic activity and reusability of ZnO arrays are beneficial for their application as regenerated catalysts.

3.4. Removal mechanism of ZnO nanorods for azo dyes

The worth mentioning is that during the degradation experiments undertaking in the dark or vis-light illumination requirement, the decoloration of the test dyes was accompanied by flocculent precipitates produced around the ZnO films. To clarify the removal mechanism of the azo dyes, the collected cardinal red flocculent precipitates from decolorized CR solution by sample Z-3, as well as the original CR dye, were characterized by XRD and FTIR. Furthermore, the regenerated sample Z-1 and Z-3 were annealed at 300 ˚C for 2 h to completely remove CR dye molecules on the surface of catalyst, followed by peeling off the ZnO layer from Zn substrate. And then the unannealed (before degradation) and annealed (after degradation) ZnO powders were analyzed by means of XPS.

A comparative combination of XRD patterns of the flocculent precipitates collected from decolorized CR solution by sample Z-3 under different lighting conditions is presented in Fig. 5, where it can be observed that both precipitates show the reflections of hexagonal wurtzite structural ZnO, which originated from ZnO nanorods breaking away from Zn substrate and dispersing in the CR solution. Notably, some minor reflections with lower intensity in the whole range are detected for the precipitates. Comparing with the CR diffraction peaks, no CR peaks are observed from the precipitates. These indicate that the ZnO catalyst does not adsorb the CR dye after the degradation reaction of CR, and the minor reflections may be ascribed to intermediate products of catalytic reaction owing to the unfinished mineralization of organic dye. Fourier transform infrared spectroscopy (FTIR) is usually employed as an additional probe to evidence the presence of OH groups as well as other organic and inorganic species. Here, we use the FT-IR technique to identify specific changes of the functional groups in the collected flocculent precipitates and CR dye molecules. From Fig. 6, one can see that no characteristic peaks of CR dye occur in the FT-IR spectrum of the precipitates dried after the catalysis reaction, which is also confirmed by the XRD analysis. It further gives evidence that the dye molecules are not adsorbed by the catalyst, implying that the degradation of the dye is caused by the catalytic reaction instead of adsorption. Besides, both XRD and FTIR peaks of the precipitates from dark condition are almost the same as those from visible light irradiation, making it clear that the degradation of CR under darkness and vis-light share identical catalytic mechanism. The similar characterization results are valid for the pale yellow flocculent precipitates collected from decolorized MO solution.

To identify the oxygen chemical states of the ZnO nanorods on Zn substrate, high resolution XPS studies were carried out. Fig. S5 (Supp. Inf.) shows the Gauss fitting curves of O1s spectra of the sample Z-1 and Z-3, respectively. Three deconvoluted peaks centered at ca. 529.6, 530.8, and 532.0 eV can be identified, which indicated that there are three sorts oxygen in the surface, the lattice oxygen ($O_{lattice}$), the adsorbed oxygen (O_x^-) and bound oxygen ($O_{adsorbates}$), respectively. The peak at 529.6 eV can be attributed to O^{2-} ion in wurtzite structure under a fully oxidized stoichiometric condition.[42,43] The lattice oxygen could not be interacted with the azo dyes, and unable to affect the formation of main charge-carrier holes in ZnO. The highest binding energy of 532.0 eV is attributed to the loosely bound oxygen on the surface of the sample, which are chemisorbed or dissociated oxygen or OH species.[42,43] The binding energy of 530.8 eV results from the absorbed O_x^- ions (O^- and O_2^- ions) in the oxygen deficient regions within the matrix of ZnO,[43-45] caused by oxygen vacancy (V_O), oxygen interstitial (O_i), and oxygen antisite (O_{Zn}).[42] The absorbed O_x^- ions are in favor of degradation reactions to promote the oxidation of organic substances.[46] For the ZnO nanorods on Zn substrate, a calculation of the area underneath the fitting curves for O1s spectra gave a percentage of absorbed O_x^- species of 37.03% and 38.05% for the sample Z-1 and Z-3, respectively. After degradation of 5 cycling runs, the absorbed O_x^- species are 36.11% and 35.68% for the sample Z-1 and Z-3, respectively. Comparing these data, one can find that there is only a little decrease of the absorbed species before and after degradation of 5 cycling runs. It illustrates that ZnO nanorods with different morphology on Zn substrate have the same oxygen chemical states, which promote the oxidation of organic substances.

It is noteworthy that the investigated dyes in our degradation experiments were not only anionic azo dyes of CR and MO but also cationic azo dyes of rhodamine B (RB) and methylene blue (MB). However, even though the aqueous cationic azo dyes with

low concentration, namely, 10^{-5} M of RB and MB solution, negligible removal efficiency could be detected in the presence of ZnO nanostructural catalysts (not show here). Therefore, ZnO arrays might be effective only for the degradation of anionic azo dyes. J.M. Wu et al[47] have reported the catalyzed degradation of anionic azo dyes in the presence of layered perovskite $La_4Ni_3O_{10}$ powders under ambient conditions without light. They demonstrated that the additive of Ag^+ in the reaction system, which serves as an electron acceptor, markedly enhanced the MO degradation rate, suggesting that MO molecules were oxidized, not reduced as is the case in the degradation tactic utilizing zero-valent iron.[48,49]

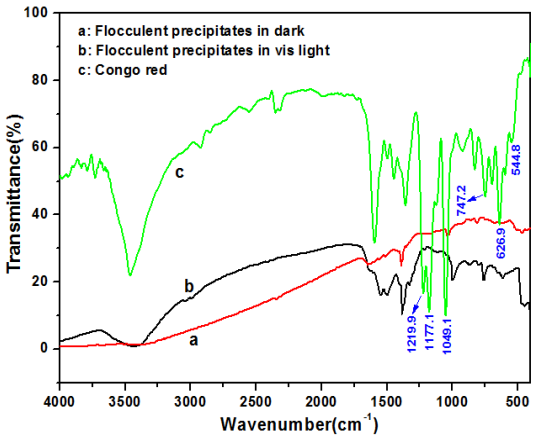

Fig. 6 FTIR spectra of the flocculent precipitates collected from the degraded CR solutions under different lighting conditions (Vis-light irradiation and dark condition).

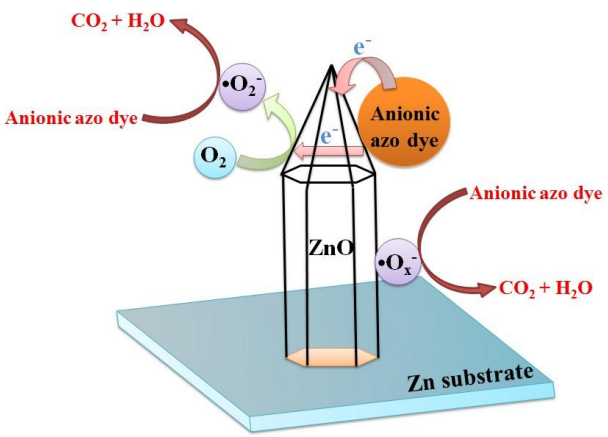

Fig. 7 Schematic illustration for the proposed catalytic degradation mechanism, and the electrons transfer from anionic azo dye to ZnO nanopencil under dark condition.

Additionally, the MO degradation was totally inhibited in the absence of dissolved O_2, which was achieved by thoroughly purging the solution with N_2. Purging the solution containing Ag^+ ions with N_2 achieved MO degradation, but at a rate lower than in the system open to air. This can be explained by the fact that Ag^+ ions play the same role as dissolved O_2 in the solution, that is, electron acceptors. They eventually drew a conclusion that $La_4Ni_3O_{10}$ served as a "bridge" for electron transfer during the reaction since a series of control experiments revealed that neither O_2 nor Ag^+ could oxide MO. These research results give hints for us to justify the catalytic property of ZnO arrays under the circumstances of darkness. On the other hand, in our experiment for ZnO hexagonal nanorods (sample Z-2), the dominating planes are the Zn-terminated (0001) plane. While for ZnO nanopencils (sample Z-3) and nanopyramids (sample Z-1 and Z-4), the dominating planes are six equivalent polar $\{10\bar{1}1\}$ planes and nonpolar $\{0\bar{1}10\}$ planes, respectively. The difference of surface atomic structures will result in a distinct ability to absorb the oxygen species (such as O^-, O^{2-}, O_2, OH^-) and target molecules. The polar $\{10\bar{1}1\}$ planes with six equivalent planes have the highest chemisorption ability and probability, and the polar (0001) plane terminated with Zn^{2+} ions comes second[50] Due to nonsaturable oxygen coordination, Zn^{2+} ions on the exposed $\{10\bar{1}1\}$ or (0001) surfaces are able to catch atmosphere oxygen (O_2) through chemical/physical absorption.[51] Thus, the $\{10\bar{1}1\}$ or (0001) surfaces terminated with Zn^{2+} ions can be easy to adsorb O_2 and objective anionic azo dye molecules in the solution condition of degradation. Based on above theories, the possible catalytic mechanism in our experiment is proposed as illustrated in Fig. 7. Taking ZnO nanopencils for example, CR or MO molecules become negatively charged organic groups through ionization in water, which are consequently adsorbed on the $\{10\bar{1}1\}$ surfaces of nanopencils. In this case, electrons from CR or MO molecules transfer to ZnO and further react with dissolved O_2 absorbed on the catalyst surface, resulting in dye degradation. If no suitable electron acceptors exist to receive the electrons, they would recombine with the dye molecules, which inhibit the degradation procedure. When the system is open to air, further deep degradation of the intermediates by the produced reactive oxygen species such as peroxide ($\cdot O_2^-$) groups is also possible, as illustrated as follows:[52]

$$\text{CR or MO} \xrightarrow{\text{ZnO}} e^- \quad (5)$$

$$O_2 + e^- \rightarrow \cdot O_2^- \quad (6)$$

$$\cdot O_2^- + H^+ \rightarrow \cdot HO_2 \quad (7)$$

$$\cdot HO_2 + H_2O \rightarrow H_2O_2 + \cdot OH \quad (8)$$

$$H_2O_2 + e^- \rightarrow \cdot OH + OH^- \quad (9)$$

$$\text{CR or MO} + \cdot OH \rightarrow \text{intermediates} \rightarrow CO_2 + H_2O \quad (10)$$

Although ZnO nanorod and nanopyramid arrays exhibit relative lower removal efficiency on the decoloration of dye when compared with ZnO with hexagonal pencil-like morphology, their intrinsic catalytic ability and reusability are, of course, non-ignorable. The inherent existence of the absorbed O_x^- ions (O^- and O_2^-) in the oxygen deficient regions within the matrix of ZnO generated during the material synthesis procedure have been proved by XPS studies, rationalizing the similar excellent degradation performance of all the ZnO nanorod samples at the initial stage of the repeated degradation experiments (the first or second cycling). As simultaneously displayed in Fig. 7, the absorbed O_x^- species take protons from aqueous solution to yield superoxide ($\cdot OH_2$) followed by the formation of hydrogen peroxide (H_2O_2). Hydrogen peroxide can split and give hydroxide radical and hydroxyl (Eqn. (7), (8) and (9)), which are strong oxidizing agents for decomposing the organic dye:

$$\cdot O_x^- + \text{CR or MO} \rightarrow \text{intermediates} \rightarrow CO_2 + H_2O \quad (11)$$

4. Conclusions

In summary, we have prepared ZnO nanorods arrays on Zn substrates with different definite crystal surfaces. The relationships between morphology and catalytic activity have been studied. The aqueous azo dyes can be degraded efficiently under ambient conditions in the presence of the ZnO nanorods arrays. The catalytic activity can be maintained for at least five runs, which is of great importance for potential practical applications. The catalytic degradation process reported herein requires no external energy input, and it can be carried out under various ambient conditions (ultraviolet light, visible light and dark), which we believe is of potential importance for the low-cost treatment of azo-dye effluents. The mechanism behind this process is also of interest for the design of novel catalysts and the related theory, which can be concluded that the catalytic activity of the ZnO samples with different morphologies depends on the chemistry sorption ability of the exposed planes. Certainly, a further study is required to clarify those factors affecting the interfacial charge transfer.

Acknowledgements

This work was supported by the Department of Science and Technology of Yunnan Province via the Key Project for the Science and Technology (Grant No.2011FA001), and National Natural Science Foundation of China (Grant No.51262029), the Key Project of the Department of Education of Yunnan Province (ZD2013006), and Program for Excellent Young Talents, Yunnan University. Igor Djerdj acknowledges financial support from the Unity through Knowledge Fund (www.ukf.hr) of the Croatian Ministry of Science, Education and Sports (Grant Agreement No. 7/13).

Notes and references

[a]*Department of Materials Science and Engineering, Yunnan University, 650091 Kunming, Peoples' Republic of China. Fax: +86-871-65153832; Tel: +86-871-65031124; E-mail: ydwang@ynu.edu.cn*
[b]*State Key Lab of Silicon Materials, Zhejiang University, Hangzhou 310027, People's Republic of China*
[c]*Ruđer Bošković Institute, Bijenička 54, 10000 Zagreb, Croatia. Fax: +38514680114; Tel: +38514680113; E-mail: igor.djerdj@irb.hr*

1. Y. Z. Zhang, J. T. Zheng, X. F. Qu and H. G. Chen, *J. Colloid Interf. Sci*., 2007, **316**, 523.
2. F. Zhang, Y. J. Liu, Y. Cai, H. Li, X. Y. Cai, I. Djerdj and Y. D. Wang, *Powder Technol*., 2013, **235**, 121.
3. T. Robinson, G. McMullan, R. Marchant and P. Nigam, *Bioresource Technol*., 2001, **77**, 247.
4. F. Zhang, Y. J. Liu, X. C. Xiao, X. Y. Cai, H. Li and Y. D. Wang, *Mater. Technol*., 2012, **27**, 196.
5. M. Q. Yang, X. Pan, N. Zhang and Y. J. Xu, *CrystEngComm*, 2013, **15**, 3022.
6. S. Liu and Y. J. Xu, *Nanoscale*, 2013, **5**, 9330.
7. Q. Xiao and C. Yao, *Mater. Chem. Phys*., 2011, **130**, 5.
8. M. Q. Yang and Y. J. Xu, *Phys. Chem. Chem. Phys.*, 2013, **15**, 19102.
9. D. Zhao, C. C. Chen, Y. F. Wang, W. H. Ma, J. C. Zhao, T. Rajh and L. Zang, *Environ. Sci. Technol*. 2008, **42**, 308.
10. Y. Zhang, Z. R. Tang, X. Fu and Y. J. Xu, *ACS Nano*, 2010, **4**, 7303.
11. N. Zhang, S. Liu and Y. J. Xu, *Nanoscale*, 2012, **4**, 2227.
12. I. Sopyan, N. Hafizah and P. Jamal, *Indian J. Chem. Technol*., 2011, **18**, 263.
13. T. Ghosh, K. Ullah, V. Nikam, C. Y. Park, Z. D. Meng and W. C. Oh, *Ultrasonics Sonochemistry*, 2013, **20**, 768.
14. A. Z. Abdullah and P. Y. Ling, *J. Hazard. Mater*., 2010, **173**, 159.
15. X. Y. Cai, Y. Cai, Y. J. Liu, S. J. Deng, Y. Wang, Y. D. Wang and I. Djerdj, *Ceram. Int*., 2014, **40**, 57.
16. C. Hariharan, *Appl. Catal. A: Gen.*, 2006, **304**, 55.
17. D. Fu, G. Han, Y. Chang and J. Dong, *Mater. Chem. Phys*., 2012, **132**, 673.
18. T. Zhai, S. Xie, Y. Zhao, X. Sun, X. Lu, M. Yu, M. Xu, F. Xiao and Y. Tong, *CrystEngComm*, 2012, **14**, 1850.
19. M. D. Hernández-Alonso, F. Fresno, S. Suárez and J. M. Coronado, *Energy Environ. Sci*., 2009, **2**, 1231.
20. N. Daneshvar, D. Salari and A. R. Khataee, *J. Photochem. Photobio. A: Chem*., 2004, **162**, 317.
21. Z. L. Wang and J. H. Song, *Science*, 2006, **312**, 242.
22. M. Law, L. E. Greene, J. C. Johnson, R. Saykally and P. Yang, *Nat. Mater*., 2005, **4**, 455.
23. X. D. Wang, C. Neff, E. Graugnard, Y. Ding, J. S. King, L. A. Pranger, R. Tannenbaum, Z. L. Wang and C. J. Summers, *Adv. Mater*., 2005, **17**, 2103.
24. X. Feng, L. Feng, M. Jin, J. Zhai, L. Jiang and D. J. Zhu, *J. Am. Chem. Soc*., 2004, **126**, 62.
25. F. Zhao, X. Li, J. Zheng, X. Yang, F. Zhao, K. Wong, J. Wang, W. Lin, M. Wu and Q. Su, *Chem. Mater*., 2008, **20**, 1197.
26. S. Ma, R. Li, C. Lv, W. Xu and X. Gou, *J. Hazard. Mater*., 2011, **192**, 730.
27. Q. Ahsanulhaq, A. Umar and Y. B. Hahn, *Nanotechnology*, 2007, **18**, 115603.
28. Y. Fang, Q. Pang, X. Wen, J. Wang and S. Yang, *Small*, 2006, **2**, 612.
29. L. Shi, K. Bao, J. Cao and Y. Qian, *CrystEngComm*, 2009, **11**, 2009.
30. P. X. Gao and Z. L. Wang, *J. Phys. Chem. B*, 2004, **108**, 7534.
31. R. A. Laudise and A. A. Ballman, *J. Phys. Chem*., 1960, **64**, 688.
32. W. J. Li, E. W. Shi, M. Y. Tian, B. G. Wang and W. Z. Zhong, *Sci. China E*, 1998, **41**, 449.
33. H. Zhang, D. Yang, Y. Ji, X. Ma, J. Xu and D. Que, *J. Phys. Chem. B*, 2004, **10**, 3955.
34. R. A. Laudise, *Englewood Cliffs, N.J.: Prentice-Hall.* 1970.
35. Y. Wang, Y. Wang, Y. L. Meng, H. M. Ding, Y. K. Shan, X. Zhao and X. Z. Tang, *J. Phys. Chem. C*, 2008, **112**, 6620.
36. Q. Wan, T. H. Wang and J. C. Zhao, *Appl. Phys. Lett.*, 2005, **87**, 83.
37. L. Di, H. Hajime, O. Naoki, N. Saito and S. Hishita, *Thin Solid Films*, 2005, **486**, 20.

38. M. R. Hoffmann, S. T. Martin, W. Choi and D. W. Bahnemann, *Chem. Rev*., 1995, **95**, 69.
39. H. Tong, S. Ouyang, Y. Bi, N. Umezawa, M. Oshikiri and J. Ye, *Adv. Mater*., 2012, **24**, 229.
40. H. Li, G. Wang, F. Zhang, Y. Cai, Y. D. Wang and I. Djerdj, *RSC Advances*, 2013, **2**, 12413.
41. B. Weng, M. Q. Yang, N. Zhang and Y. J. Xu, *J. Mater. Chem. A*, 2014, **2**, 9380.
42. M. Chen, Z. Wang, D. Han, F. Gu and G. Guo, *J. Phys. Chem. C*, 2011, **115**, 12763.
43. J. C. Lin, K. C. Peng, H. L. Liao and S. L. Lee, *Thin Solid Films*, 2008, **516**, 5349.
44. M. Chen, X. Wang, Y. H. Yu, Z. L. Pei, X. D. Bai, C. Sun, R. F. Huang and L. S. Wen, *Appl. Surf. Sci*., 2000, **158**, 134.
45. J. Wang, Z. Wang, B. Huang, Y. Ma, Y. Liu, X. Qin, X. Zhang and Y. Dai, *ACS Appl. Mater. Interfac*., 2012, **4**, 4024.
46. H. Liu, S. Cheng, M. Wu, H. Wu, J. Zhang, W. Li and C. Cao, *J. Phys. Chem. A*, 2000, **104**, 7016.
47. J. M. Wu and W. Wen, *Environ. Sci. Technol*., 2010, **44**, 9123.
48. J. A. Mielczarski, G. M. Atenas and E. Mielczarski, *Appl. Catal. B*: *Environ*., 2005, **56**, 289.
49. A. D. Bokare, R. C. Chikate, C. V. Rode and K. M. Paknikar, *Appl. Catal. B*: *Environ*., 2008, **79**, 270.
50. X. G. Han, H. Z. He, Q. Kuang, X. Zhou, X. H. Zhang, T. Xu, Z. X. Xie and L. S. Zheng, *J. Phys. Chem. C*, 2009, **113**, 584.
51. J. Yang, J. Wang, X. Li, J. Lang, F. Liu, L. Yang, H. Zhai, M. Gao, X. Zhao, *J. Alloys Compounds*, 2012, **528**, 28.
52. G. K. Pradhan and K. M. Parida, *J. Eng. Sci. Technol*., 2010, **2**, 53.

Graphical Abstract

ZnO nanorods arrays on Zn substrates with different definite crystal surfaces can efficiently degrade azo dyes (Congo red and methyl orange) under ambient conditions, requiring neither light illumination nor additional energy (agitation, ultrasonic, etc.).